Comparison of Length and Transport of Entrapped Woody Debris in Coniferous and Broadleaf Forests Based on Mapping Using Ortho-Photographs Acquired by Uncrewed Aerial Vehicle

Haruka Tsunetaka (tsunetakaharuka@ffpri.affrc.go.jp)
Forestry and Forest Products Research https://orcid.org/0000-0001-7831-6193
Slim Mtibaa
57880-Forestry and Forest Products Research Institute
Shiho Asano
57880-Forestry and Forest Products Research Institute
Takashi Okamoto
57880-Forestry and Forest Products Research Institute
Ushio Kurokawa
57880-Forestry and Forest Products Research Institute

Research article

Keywords: UAV, Woody debris, Debris flow, Landslide

Posted Date: August 31st, 2020

DOI: https://doi.org/10.21203/rs.3.rs-67734/v1

Version of Record: A version of this preprint was published on March 26th, 2021. See the published version at https://doi.org/10.1186/s40645-021-00419-6.

Abstract

Landslides and debris flows often result in woody debris from initiation and riparian zones, through their runout. Considering that woody debris is one of the main components of watershed ecosystems, the importance of quantifying its properties and transport is evident. However, the low accessibility of disturbed channels after landslides and debris flows generally impedes the accurate and quick investigation of woody debris. The recent advances in photogrammetry techniques and technology may overcome such issues. In this study, we used ortho-photographs acquired by a small uncrewed aerial vehicle (UAV) for measuring the lengths of woody debris entrapped mainly by closed-type check-dams. We focused on two channels, located in coniferous and broadleaf forests and affected by two different landslides events. The measurement accuracy was analyzed by comparing the lengths derived from the UAV method with direct measurements. When both edges of woody debris were satisfactorily extracted from an ortho-photograph acquired via UAV, the length of the woody debris with respect to coniferous trees can be measured with an accuracy of approximately ±0.5 m. However, some coniferous trees were captured by stand trees in the riparian zone, and the coverage by tree-crowns led to the underestimation by several meters of the extracted length of the entrapped woody debris. For broadleaf trees, most of the extracted lengths were shorter than the directly measured lengths. This is probably caused by the low visibility of both edges due to the complex structures of the root-wad and the tree-crown. Our results showed that there were no significant changes in the lengths and locations of the entrapped woody debris, in both sites, after seven months of the first UAV flight. In the coniferous forests, the rainfall that triggered landslides in 2017 exceeded the 100-year return level, which was obviously an abnormal intense rainfall. Although the 2019 rainfall event that occurred between UAV flights was not as much to the rainfall triggering landslides, rainfall intensities with different durations reached the second-highest value from 1976 to 2019, exceeding the 30-years return period. This suggests that most of the entrapped woody debris rarely migrate even under extreme rainfall.

Introduction

Debris flow causes entrainment of stand-woods located in the initiation and riparian zones, and, consequently, may include dozens of percentage of woody debris by volume (Johnson et al., 2000; May and Gresswell, 2003a; Lancaster et al., 2003). In addition to its destructive impact on life and infrastructure (e.g., Ruiz-Villanueva et al., 2013), woody debris in debris flow can alter the flow regime because of their irregular shape that can be entrapped around obstacles, leading to anomalous deposition of sediment and inundations (e.g., May, 2002; Lancaster et al., 2003; Tang et al., 2018; Booth et al., 2020). Therefore, the accumulation of woody debris results in structural peculiarities around the channel networks (e.g., Keller and Swanson, 1979; Woodsmith and Buffington, 1996; Montgomery et al., 1996; Nakamura and Swanson, 2003). This contributes to changes in the ecosystem, the channel morphology, and the sediment flux through woody-debris preservation and decay (e.g., Wallace and Benke, 1984; Lisle, 1995; Montgomery et al., 1995; Gurnell et al., 2001; Comiti et al., 2006; Ruiz-Villanueva et al., 2016). Hence, the river form and function are determined by the interaction between water,

sediment, and wood (Nakamura et al., 2017; Swanson et al., 2020). Quantifying woody debris is important for assessing its impacts on ecological, geomorphological, and fluvial conditions.

Many previous studies focusing on in-situ channels have contributed to unraveling the role of woody debris in various spatiotemporal-scales and environmental settings, but most of these approaches required direct field measurements, such as local monitoring (e.g., Manners et al., 2007), tracking of woody debris (e.g., Ravazzolo et al., 2015; Wyżga et al., 2017), and field experiments using artificial woody debris (e.g., Haga et al., 2002). Taking into account the diversity of forests around channels (e.g., age, species, and density of trees), the accumulation of field data is obviously an effective approach. However, the necessity of human effort in the field hinders data acquisition at inaccessible areas (e.g., headwater channels and disturbed areas immediately after landslides and debris flows). In practice, the field data acquisition is difficult for a large scale area exceeding a sub-basin size. The improvement of field measurement techniques with respect to woody debris remains a critical issue.

To address the measurement issues of woody debris, remote sensing approaches using three-dimensional data have been applied. The Use of LiDAR (light detection and ranging) data clearly reduces the processing time required for mapping the logjam and large woody debris (Kasprak et al., 2012; Abalharth et al., 2015; Atha and Dietrich, 2016). However, such technology is expensive and therefore available only in some regions. Alternatively, photogrammetry based on structure from motion multi-view stereo (SfM-MVS) using UAV (uncrewed aerial vehicle) has been proven time-efficient compared to classical field surveys (Sanhueza et al., 2019). This approach overcomes data availability issues and is relatively low-cost. Nevertheless, most tests were conducted in low-land and flood plains rather than low-accessibility areas such as steep channels (e.g., Sanhueza et al., 2019). As the accuracy of SfM-MVS is remarkably influenced by complex surfaces and obstacles, such as steep slopes, large reliefs, and vegetation coverage (e.g., Fonstad et al., 2013; James and Robson, 2014), many unresolved uncertainties remain over the application of the SfM-MVS approach in steep and complex targets, such as woody debris in channels.

Aerial photography being one of the traditional two-dimensional data sources may more or less provide meaningful information on woody debris. Even satellite images from Google Earth are being used as accurate for mapping woody debris (Atha, 2013; Ulloa et al., 2015). Hence, the efficacy of aerial photography is evident, but the accuracy and effort of mapping depend on the image quality. In this respect, it is expected that small UAVs allow acquiring high-resolution aerial photographs at low cost because of the lower flight-altitude and higher portability compared to conventional aerial vehicles. Moreover, because flights of small UAVs can overcome inaccessibility issues and cover several kilometers depending on the flight design, it is a fairly attractive tool for obtaining woody debris measurements in low-accessibility areas.

In addition, although entrapped woody debris is often quickly removed to avoid unexpected damages in the downstream area due to its transport, UAV flights can be carried out immediately after rainfall events that result in a large amount of woody debris. Conversely, the risk of secondary impacts arising from

woody debris entrapment has not been evaluated properly so far, because it has been difficult to conduct field surveys immediately after intense rainfall involving woody debris supply. Therefore, mapping woody debris would enable investigating the possibility of woody debris transport due to subsequent rainfall, even if it is carried out based on a simple method using aerial photography. Nevertheless, the potential to measure woody debris based on aerial photographs acquired via UAV has not been thoroughly examined due to lack of sample cases.

In this study, we analyze the accuracy of UAV-based measurements in the case of entrapped woody debris. Two regions are selected representing two forest types, coniferous and broadleaf forests. In both regions, large amounts of woody debris were supplied through landslides and debris flows triggered by a single rainfall event. This research has two main objectives: (1) to analyze the capability of ortho-photographs acquired via UAV to measure the lengths of entrapped woody debris, and (2) to investigate the transport potential of entrapped woody debris based on rainfall analysis. Based on the results, we discuss the effectiveness of UAV measurements and how woody debris behave after their entrapment.

Study Site

To examine the influence of tree type on the measurement accuracy of woody debris using the ortho-photographs acquired by UAV, two different sites covered by coniferous or broadleaf forests were selected as study sites (Fig. 1a). Hereafter, the former site is referred to as the CF (coniferous forests) site (Fig. 1b), while the latter site is referred to as the BF (broadleaf forests) site (Fig. 1c).

Coniferous forests site

The CF site is a sub-watershed of the Otoishi watershed located in the northern part of the Kyusyu Island, Japan (Fig. 1a, b). Its highest point is about 385 m a.s.l., and its lowest point is about 225 m a.s.l. The total length of the main channel is approximately 760 m with an average slope of around 12° (before the debris flow occurrence), and the drainage area is about 0.15 km^2. To prevent hillslopes and banks destabilization, five closed-type check-dams were constructed before the debris flow occurred in 2017 (Fig. 2a). Most hillslopes are covered with artificial coniferous forests that consist mainly of *Cryptomeria japonica* and *Chamaecyparis obtusa*. The tree height ranges from about 15 to 25 m.

In the region around the CF site, the intense rainfall on July 5, 2017, triggered more than 2,000 landslides, which resulted in debris flow propagations and therefore a great amount of woody debris (Chigira et al., 2018). The sliding sediment layers were mainly granodiorite and pelitic schist (Chigira et al., 2018). The intense rainfall in July 2017 triggered seven landslides at the CF site (Fig. 2a), but the existing check-dams effectively prevented the descent of sediment and woody debris. Hence, most of the woody debris was trapped around the check-dams and along the channel, preventing the damages in the downstream residential area. Because of this low impact on the residences, woody debris had been maintained approximately untouched until the time we carried out observations.

Broadleaf forests site

The BF site is located in the Hiroshima prefecture, the west part of Japan (Fig. 1c). Here, two channels are confluent at an irrigation pond that is located at the lower end of channels (~ 305 m a.s.l., Fig. 2b). The highest points of channels A and B are ~ 410 and ~ 480 m a.s.l., respectively. Their total lengths are ~ 880 and ~ 466 m, respectively. The average slope of both channels is similar at ~ 11–12° (before the debris flow occurrence). The drainage areas of channels A and B are ~ 0.07 and ~ 0.13 km^2, respectively. Similar to the case of the CF site, four closed-type check-dams have been constructed before the debris flow occurred in 2018 (Fig. 2b). The forest type is completely different, and most of the hillslopes are covered by broadleaf forests with various tree types. The tree height ranges from about 10 to 20 m.

In the Hiroshima prefecture, the stationary front affected by Typhoon Prapiroon caused heavy rainfall on July 5–7, 2018 (Tsuguti et al., 2019) and triggered approximately 8,000 landslides due to the vulnerable geological setting mainly dominated by weathered granite (Kaibori et al., 2018). Five landslides occurred at the BF site, but the check-dams and the pond effectively prevented the descent of sediment and woody debris. Similar to the situation of the CF site after the disaster, the woody debris produced in the BF site had been almost remained untouched until we carried out the observations.

Methods

This study consists of two parts: (1) accuracy assessment of the woody debris measurement by ortho-photography acquired via UAV, and (2) rainfall analysis to investigate the possible transport of entrapped woody debris.

UAV flights and aerial-photograph processing

Two UAV flights were conducted in the study sites (Table 1). A small UAV (DJI Mavic 2 pro; Table 2) was used for the flights, covering the channel and landslides (Fig. 2). The flights were conducted manually at elevations between about 50 m and 200 m, and most of the photographs were taken in nadir direction. The flight path accounted for an overlap in the aerial-photographs of at least 70%. To reduce differences in shade and brightness among the acquired aerial-photographs, the flights were operated by avoiding the strong sunlight.

Table 1
Properties of UAV and the installed camera.

UAV	
Model	DJI Mavic 2 pro
Weight	907 g
Diagonal size	354 mm
Max. duration of flight	31 min
Camera	
Number of pixels	20 M
Senser size	13.2 × 8.8 mm
Focal length	∞

Table 2
Date of UAV flights and number of aerial photographs to provide ortho-photographs

	Date	**Number of aerial photographs**
CF site		
First flight	February 14, 2019	159
Second flight	September 26, 2019	284
BF site		
First flight	November 16, 2018	315
Second flight	December 25, 2019	141

The acquired photographs were processed using the SfM-MVS photogrammetry software (Agisoft, Metashape Professional version 1.5.1). In most cases, immediately after debris flow disaster, woody debris generally impede the setting of ground control points (GCPs) as they behave as obstacles. Considering this, our intention was to assess the accuracy of measurements using only UAV flights (without any other field operations). Hence, the position data of a built-in GNSS (global navigation satellite system) contained in exchangeable image file format data of each photograph was used for geo-referencing. Following the standard SfM-MVS photogrammetry workflow, without geo-referencing using GCPs, the ortho-photographs were produced with a spatial resolution of 0.03–0.05 m.

Because the processing was performed without georeferencing by GCPs, the coordinates of the resulted ortho-photographs taken during the different flight dates did not overlap. As the aim of using sequential ortho-photographs is to investigate the possible migration of the entrapped woody debris, it is necessary

that the relative coordinate system overlap, even if the absolute coordinate system did not. Thus, we manually adjusted two sequential ortho-photographs by using the crests of the check-dams as reference points, whose coordinates were taken from the older ortho-photograph. Using the extracted coordinates, the ortho-photograph acquired on the later date was transformed to fit the first one. The differences in lengths regarding selected the immobilized objects (e.g., large boulders and crests of check-dams) were less than about 0.2 m. Therefore, the horizontal accuracy of ortho-photographs was considered as less than a few decimeters.

Accuracy assessment

First, the length of entrapped woody debris was extracted as line data from ortho-photographs. The measurement accuracy of the extracted length is presumably affected by visibility, which is related to the types and sizes of the trees. Moreover, because woody debris is often inclined and broadleaf trees have a curved shape, the orthogonal projection in the extracted length possibly causes a measurement error (Fig. 3). Hence, we focused on the differences due to tree types, diameter, and entrapment inclination of the woody debris. In the selected woody debris, the length excluding the root-wad and twigs was directly measured and compared with the extracted length (Fig. 3). The diameters of the woody debris were measured at about 1.0 to 1.5 m height from the root-wad. For small woody debris of less than about 1.5 m, because the difference in the thickness of a single fragment was slight, we measured the diameter at an arbitrary location. In the CF site, as woody debris remained relatively straight shape, the entrapment inclination was directly measured (Fig. 3b). The results of direct measurements were compared with the length extracted from the ortho-photographs of the first UAV flight.

The extraction of woody debris depends on its visibility in the ortho-photographs, and thus the identification of its origin as well as the detection of small woody debris would go beyond the measurement purpose. Moreover, the extracted woody debris may contain multiple fragments that originated from a single tree. In other words, as a single stand-wood may result in several batches of woody-debris, counting the extracted woody debris involves uncertainty. Considering this unavoidable risk of over- or under-estimation in the amount of woody-debris, we avoided a detailed interpretation and analysis using the extracted numbers of woody-debris.

Analysis to determine the transport of woody debris

To analyze whether or not woody debris migrated through time, we created quantile-quantile (Q-Q) plots with respect to the probability density of the extracted length. The CF site was divided into seven regions, six landslide scars and the riparian zone (Fig. 2a). Accordingly, changes in the probability density of the woody debris length were visually tested using the Q-Q plots. Similarly, Q-Q plots were made for the channels A and B of the BF site (Fig. 2b). For each region, to investigate the coincidence of the probability density of the extracted length between the two flight dates, a goodness-of-fit test was carried out using the Kolmogorov–Smirnov test.

In addition, we investigated whether specific rainfall characteristics triggered the secondary transport of woody debris. For this reason, we used the hourly rainfall records from 1976 to 2019 obtained at the

closest rain-gauges installed by the Japan Meteorological Agency, the Asakura station (for the CF site, Fig. 1b) and Higashihiroshima station (for the BF site, Fig. 1c). The annual maxima of rainfall intensity with various durations (1, 2, 3, 6, 12, 24, 48, and 72 hours) were investigated from 1976 to 2019 and compared with the intensity of the rainfall that triggered the debris flow. In addition, we examined records of rainfall maxima after the debris-flow occurrence. The return periods were calculated based on the probability density of each rainfall intensity fitted by the Gumbel distribution based on the annual maxima (e.g., Koutsoyiannis et al., 1998; Sane et al., 2018). For this fitting process, the goodness-of-fit test (Kolmogorov–Smirnov test) resulted in *p*-values exceeding 0.1, suggesting that the applied Gumbel distribution models fitted the probability density of the observed rainfall well.

Results

Length of the entrapped woody debris

As expected, the comparison between the extracted and measured length of the woody debris indicates that the measurement accuracy depends on the visibility of the woody debris entrapments. Fifty batches of woody debris were directly measured at the CF site (Fig. 4a). Fourteen of them were trapped by stand-woods located in the riparian zone, and they were partially invisible from the sky due to the coverage by the tree crown. This low visibility caused underestimation of the extracted length, with errors in length at a maximum of ~ 10 m. By contrast, 36 other batches were fully visible, and their lengths ranged between about 3 m and 22 m. Despite this wide range, most measurements coincided well with the extracted lengths. This clear dependency on the visibility of woody debris was reflected in the box-plot (Fig. 5), indicating that the interquartile ranges obviously differed between visible and covered woody debris; the differences were from − 0.4 to 0.5 m and from 1.6 to 4.3 m, respectively (Fig. 5).

The length of 130 woody debris batches without crown coverage was directly measured at the BF site but rarely coincided with the extracted length, which was usually an underestimation (Fig. 4b). Moreover, the differences between the lengths varied. The related interquartile range ranged between about 0.3 m and 2.1 m, reflecting low accuracy and high uncertainty in the measurement of broadleaf trees compared to coniferous trees (Fig. 5).

Strictly speaking, the extracted length was the orthogonally projected length, and therefore, we calculated the slope distance of the measured woody debris from the extracted length using the measured slope. However, this correction did not significantly improve the measurement accuracy because differences in the visibility of the woody debris and the tree types overwhelmed the influence arising from the approximation by the orthogonal projection (Figs. 4a and 6). The differences in the diameter of the woody debris indicate that the extracted length of relatively narrow batches (< ~ 0.2–0.3 m in diameter) tends to be underestimated (Fig. 7), suggesting that it depends on visibility.

At the CF site, the interquartile ranges slightly differ among the landslide scars, but they are similar between the riparian zone and the average of all landslides, which is 2.5 to 7.7 m and 2.6 to 8.3 m,

respectively (Fig. 8a). The length median of the woody debris ranged from 3.4 m (in landslide 4) to 7.8 m (in landslide 1). At the BF site, the interquartile ranges of the length of the woody debris at the check-dams A and B were 1.1 to 3.1 m and 0.8 to 2.6 m, respectively (Fig. 8b). The medians of the check-dams A and B were similar, 1.8 m and 1.5 m, respectively. Consequently, the length median of the woody debris at the CF site was ~ 4.5 m and obviously greater than that at the BF site (Fig. 8c).

Transport of entrapped woody debris

At both sites, the visible changes in the spatial distribution of the woody debris between the two ortho-photographs were slight (Figs. 9 and 10). Woody debris was trapped in various areas, for instance, as stand-woods in the riparian zone, the check-dams, and the landslide areas. Despite these differences in the entrapment regions, most of the woody debris seems did not move even after about 7 months (at the CF site, Fig. 9) and over one year (at the BF site, Fig. 10). The Q-Q plots indicate that the probability density of the extracted woody debris length coincided well with the measured length, regardless of the division of the entrapment regions (Fig. 11). Thus, the *p*-values with respect to the goodness-of-fit test exceeded 0.05, suggesting that the changes were statistically small.

The rainfall anomalies that triggered debris flows were revealed by comparing the annual maxima of the rainfall intensity in each case. At the CF site, the rainfall that triggered debris flow in 2017 was obviously excessive rainfall, as the rainfall intensity was the highest compared with the annual maxima of other years, regardless of the rainfall duration (Fig. 12a). This suggests that the highly intense and continuous rainfall resulted in the large amount of woody debris. At the BF site, regarding the rainfall that triggered debris flows in 2018, rainfall intensities with 1–6 hours durations were not higher than the other annual maxima since 1976, but those with 12–72 hours durations were the most intense since 1976 (Fig. 12b). This suggests that the high rainfall intensity continuing over 12-hours resulted in landslides and debris flow with the propagation of woody debris. Both rainfall events that triggered debris flows at the CF and BF sites reached the level exceeding the 100-years return period (Tables 3 and 4).

Table 3
Return period (*RP*) for annual maxima of rainfall intensities in the CF site.

	RP_{1h}	RP_{2h}	RP_{3h}	RP_{6h}	RP_{12h}	RP_{24h}	RP_{48h}	RP_{72h}
	(year)							
2017	> 100	> 100	> 100	> 100	> 100	> 100	> 100	> 100
2018	1.66	2.68	3.47	10.84	17.60	20.70	33.67	17.05
2019	10.32	11.98	14.18	33.46	32.22	15.86	11.17	11.31

Table 4
Return period (*RP*) for annual maxima of rainfall intensities in the BF site.

	RP_{1h}	RP_{2h}	RP_{3h}	RP_{6h}	RP_{12h}	RP_{24h}	RP_{48h}	RP_{72h}
	(year)							
2018	15.60	14.67	11.88	13.70	> 100	> 100	> 100	> 100
2019	3.77	2.76	1.90	2.36	2.13	2.00	1.77	1.67

At the BF site, after the landslides and debris flow in 2018, the annual rainfall intensity maxima in 2019 was not remarkable (Fig. 12b, Table 4). Thus, it is difficult to analyze the potential of secondary transport of entrapped woody debris via intense rainfall. By contrast, at the CF site, after the landslides and debris flow in 2017, the annual rainfall intensity maxima in 2018 and 2019 were the second or third highest values since 1976 (Fig. 12a). Although the intensity of the triggering rainfall in 2017 significantly exceeded the annual maxima in 2018 and 2019 in terms of the return period, some rainfall intensities in 2018 and 2019 exceeded the level of the 30-years return period (Table 3). Such a heavy rainfall event occurred for example on July 21, 2019 (in between the UAV flights at the CF site; Table 2).

Discussion

Implications for UAV-based woody debris mapping

Our results demonstrate that the visibility and tree types of the woody debris determine the ability to accurately measure the length of the woody debris using ortho-photographs acquired via UAV. The length of most of the woody debris batches originating from coniferous trees was measured with less than ± 0.5 m accuracy using the ortho-photograph acquired by UAV, whereas in the case of broadleaf trees the length was underestimated systematically despite the absence of tree-crown coverage lowering visibility (Figs. 4b and 5). Considering the complex structures of both ends of broadleaf trees (i.e., wide and rounded crown and root-wad; Fig. 3b), this underestimation may be attributed to missing extractions due to low visibility of the broadleaf trees arising from complex structures at the ends. In addition, the length of the entrapped woody debris at the BF site was less than that at the CF site (Fig. 8), implying the fragmentation of broadleaf trees during the debris flow. Although the characteristics of debris flow also probably influence the magnitude of woody debris fragmentation (e.g., Johnson et al., 2000; Lancaster et al., 2003), the fragility of broadleaf trees may reduce the measurement accuracy based on the ortho-photograph at the BF site by decreasing the visibility of woody debris.

Hence, most of the factors that decrease the measurement accuracy of woody debris depend on visibility. Based on this interpretation, woody debris measurement via UAV has both positive and negative aspects. Several components affecting the quality of the aerial photographs (e.g., black shadow, brightness involving overexposure, and overlap ratio among aerial photographs) depend on the weather conditions and the flight plan (e.g., path, height, and direction of shooting). An adequate flight plan may significantly

improve the accuracy of UAV-based woody debris measurements. Moreover, the recently developed high-accuracy built-in GNSS-based direct geo-referencing in the SfM-MVS photogrammetry processing makes it possible to add accurate absolute coordinates without GCPs (e.g., Carbonneau and Dietrich, 2017). As part of our analysis includes manually adjusting the coordinates, this improvement is also expected to increase the measurement accuracy.

In addition, our results reveal an obvious limitation of ortho-photograph-based measurements. In general, woody debris is not only dispersedly distributed along a channel, but also results in logjam due to stacking and accumulating (e.g., Manners et al., 2007; Abalharth et al., 2015). However, the correlation between measurement accuracy and visibility from the sky demonstrates that quantitative analysis of logjam is beyond the scope of ortho-photograph-based measurements. Consequently, the total amount of woody debris is probably underestimated in all cases.

Possibility of the transport of the entrapped woody debris

The slight changes in the length and spatial distribution of the woody-debris suggest that the woody debris batches, entrapped by the check dams, did not move after the debris flow disaster (Figs. 9, 10, and 11). The elapsed time from the first flight was about seven months for the CF site and over a year for the BF site (Table 2), which may be insufficient to cause significant visible decay. This means that intact woody debris still remains in the upper regions of the channels. However, considering the slight differences in the spatial distribution and the Q-Q plot of the woody debris at the CF site (Figs. 9 and 11), the extremely high rainfall intensities in 2019 (Fig. 12a and Table 3) suggest that most of the entrapped woody debris remain in place and rarely migrate, even when intense rainfall exceeding the level of the 30-years return period occurs. This implies that most of the rainfall events that do not cause debris flows and landslides cannot trigger secondary transport of entrapped woody debris.

Because the pre-existing check-dams trapped woody debris at both sites, differences in the trend between such artificial trapping and natural entrapment of woody debris should be noted. Even so, the low transportability of the entrapped woody debris provides insight into the role of the supplied woody debris and sediment in the upstream channel after debris flows and landslides. The efficacy of woody debris trapping by closed-type check-dams is generally considered relatively low compared with the case of open-type check-dams (e.g., Piton and Recking, 2016). Nevertheless, the efficacy of woody debris trapping by closed-type check-dams was gained with long-term due to the low possibility of secondary transport. As a consequence, this low transportability of entrapped woody debris implies low erosion and discharge rate of the stored sediment, indicating that woody debris can increase sediment storage in headwater channels (e.g., May and Gresswell, 2003b). This therefore suggests that the trapping woody debris and sediment is most important for preventing their descent.

Conclusions

We mapped the entrapped woody debris using ortho-photographs acquired by UAV in two headwater channels covered by coniferous or broadleaf forests to: (1) determine whether or not ortho-photography

acquired vis UAV allows measuring the length of entrapped woody debris, and (2) investigate the possibility of transport of the entrapped woody debris by intense rainfall.

At the CF site, comparing the directly measured length with the length extracted by the UAV mapping indicates that aerial photography measurements have approximately ± 0.5 m accuracy, when both edges of the woody debris batch were satisfactorily confirmed. In contrast, some woody debris batches were trapped by stand-woods in the riparian zone, which were invisible underneath the tree crowns, and this led to underestimation of the extracted length. At the BF site, most of the extracted length values are shorter than the length measured directly, probably due to low visibility of the batch edges due to complex tree structures in the root-wad and the tree crown. Hence, these results suggest that the measurement accuracy of woody debris via UAV strongly depends on the visibility of the woody debris arising from tree types.

At both sites, changes in the frequency distribution of the length and the location with respect to entrapped woody debris were slight even over seven months had passed since the first mapping. Nevertheless, at the CF site, some rainfall intensities between the two flights reached the second-highest value since 1976. Although the rainfall intensity that triggered landslides in 2017 was higher than the annual maxima in 2019, some intensity values in 2019 exceeded the 30-years return period. This suggests that most of the entrapped woody debris remain and rarely migrate again, even under intense rainfall.

Abbreviations

BF: Broadleaf forest; CF: Coniferous forest; GCP: Ground control point; GNSS: Global navigation satellite system; LiDAR: Light detection and ranging; SfM-MVS: Structure from motion multi-view-stereo; UAV: Uncrewed aerial vehicle

Declarations

Availability of data and material

The data used in this paper are available from the authors upon request.

Competing interests

The authors declare that they have no competing interest.

Funding

This work was supported by the project “Development of technology for impacts, mitigation and adaptation to climate change in the sectors of agriculture, forestry and fisheries” of the Agriculture, Forestry and Fisheries Research Council.

Authors' contributions

HT conducted field measurements using a UAV and data analysis, and drafted this manuscript. SM conducted field measurements and rainfall processing. SA, TO, and UK carried out field measurements. All authors read and approved the final manuscript.

Acknowledgements

The authors are grateful to the staffs of Forest Agency, Japan, for their assistance in the field observations.

References

1. Abalharth M, Hassan M, Klinkenberg B, Leung V, McCleary R (2015) Using LiDAR to characterize logjams in lowland rivers. Geomorphology 246:531–541
2. Atha JB (2013) Identification of fluvial wood using Google Earth. River Research Applications 30(7):857–864
3. Atha JB, Dietrich JT (2016) Detecting fluvial wood in forested watersheds using LiDAR data: a methodological assessment. River Research Applications 32(7):1587–1596
4. Booth AM, Sifford C, Vascik B, Siebert C, Buma B (2020) Large wood inhibits debris flow runout in forested southeast Alaska. Earth Surf Proc Land 45:1555–1568
5. Carbonneau PE, Dietrich JT (2017) Cost-effective non-metric photogrammetry from consumer-grade sUAS: implications for direct georeferencing of structure from motion photogrammetry. Earth Surf Proc Land 42:473–486
6. Chigira M, Ling S, Matsushi Y (2018) Landslide disaster induced by the 2017 northern Kyushu rainstorm. Disaster Prevention Research Institute Annals A 61:28–35 (in Japanese, with English abstract)
7. Comiti F, Andreoli A, Lenzi MA, Mao L (2006) Spatial density and characteristics of woody debris in five mountain rivers of the dolomites (Italian Alps). Geomorphology 78(1):44–63
8. Fonstad MA, Dietrich JT, Courville BC, Jensen JL, Carbonneau PE (2013) Topographic structure from motion: a new development in photogrammetric measurement. Earth Surf Proc Land 38(4):755–766
9. Gurnell AM, Petts GE, Hannah DM, Smith BPG, Edwards PJ, Kollmann J, Ward JV, Tockner K (2001)ã□□Riparian vegetation and island formation along the gravel-bed Riume Tagliamento, Italy.ã□□Earth Surface Processes and Landforms 26:31–62
10. Haga H, Kumagai T, Otsuki K, Ogawa S (2002) Transport and retention of coarse woody debris in mountain streams: an in situ field experiment of log transport and a field survey of coarse woody debris distribution. Water Resource Research 38(8):1-1-1–16
11. James MR, Robson S (2014) Mitigating systematic error in topographic models derived from UAV and ground-based image networks. Earth Surf Proc Land 39:1413–1420

12. Johnson AC, Swanston DN, McGee KE (2000) Landslide initiation, runout, and deposition within clearcuts and old-growth forests of Alaska. J Am Water Resour Assoc 36:17–30
13. Kaibori M, Hasegawa Y, Yamashita Y, Sakida H, Nakai S, Kuwada S, Hiramatsu S, Jitousono T, Irasawa M, Shimizu O, Imaizumi F, Nakatani K, Kashiwabara Y, Kato N, Torita E, Hirakawa Y, Yoshinaga S, Tanaka K, Hayashi S (2018) Sediment related disaster due to heavy rainfall in Hiroshima prefecture in July, 2018. Journal of the Japan Society of Erosion Control Engineering 71(5):43–53 (in Japanese, with English abstract)
14. Kasprak A, Magilligan FJ, Nislow KH, Snyder NP (2012) A Lidar-derived evaluation of watershed-scale large woody debris sources and recruitment mechanisms: coastal Maine, USA. River Research Applications 28:1462–1476
15. Keller EA, Swanson FJ (1979) Effects of large organic material on channel form and fluvial processes. Earth Surface Processes 4:361–380
16. Koutsoyiannis D, Kozonis D, Manetas A (1998) A mathematical framework for studying rainfall intensity-duration-frequency relationships. J Hydrol 206(1–2):118–135
17. Lancaster ST, Hayes SK, Grant GE (2003) Effects of wood on debris flow runout in small mountain watersheds. Water Resour Res 39(6):1168
18. Lisle TE (1995) Effects of coarse woody debris and its removal on a channel affected by the 1980 eruption of Mount St. Helens, Washington. Water Resour Res 31:1797–1808
19. Manners RB, Doyle MW, Small MJ (2007) Structure and hydraulics of natural woody debris jams. Water Resour Res 43:W06432
20. May CL (2002) Debris flows through different forest age classes in the central Oregon Coast Range. J Am Water Resour Assoc 38(4):1097–1113
21. May CL, Gresswell RE (2003a) Large wood recruitment and redistribution in headwater streams in the Southern Oregon Coast Range, USA. Can J For Res 33:1352–1362
22. May CL, Gresswell RE (2003b) Processes and rates of sediment and wood accumulation in headwater streams of the Oregon Coast Range, USA. Earth Surf Proc Land 28:409–424
23. Montgomery DR, Buffington JM, Smith R, Schmidt K, Pess G (1995) Pool spacing in forest channels. Water Resour Res 31:1097–1105
24. Montgomery DR, Abbe TB, Peterson NP, Buffington JM, Schmidt K, Stock JD (1996) Distribution of bedrock and alluvial channels in forested mountain drainage basins. Nature 381:587–589
25. Nakamura F, Swanson FJ (1993) Effects of coarse woody debris on morphology and sediment storage of a mountain stream system in western Oregon. Earth Surf Proc Land 18:43–61
26. Nakamura F, Seo J-Il, Akasaka T, Swanson FJ (2017) Large wood, sediment, and flow regimes: Their interactions and temporal changes caused by human impacts in Japan. Geomorphology 279:176–187
27. Piton G, Recking A (2016) Design of sediment traps with open check dams. woody debris, II
28. Journal of Hydraulic Engineering 142(2):1–17

29. Ravazzolo D, Mao L, Picco L, Lenzi MA (2015) Tracking log displacement during floods in the Tagliamento River using RFID and GPS tracker devices. Geomorphology 228:226–233
30. Ruiz-Villanueva V, Bodoque JM, Díez-Herrero A, Eguibar MA, Pardo-Igúzquiza E (2013) Reconstruction of a flash flood with large wood transport and its influence on hazard patterns in an ungauged mountain basin. Hydrol Process 27(24):3424–3437
31. Ruiz-Villanueva V, Piégay H, Gurnell AM, Marston RA, Stoffel M (2016) Recent advances quantifying the large wood dynamics in river basins: New methods and remaining challenges. Rev Geophys 54(3):611–652
32. Sane Y, Panthou G, Bodian A, Vischel T, Lebel T, Dacosta H, Quantin G, Wilcox C, Ndiaye O, Diongue-Niang A, Kane MD (2018) Intensity–duration–frequency (IDF) rainfall curves in Senegal. Nat Hazards Earth Syst Sci 18:1849–1866
33. Sanhueza D, Picco L, Ruiz-Villanueva V, Iroumé A, Ulloa H, Barrientos G (2019) Quantification of fluvial wood using UAVs and structure from motion. Geomorphology 345:106837
34. Swanson FJ, Gregory SV, Iroumé A, Ruiz-Villanueva V, Wohl E (2020) Reflection on the history of research on large wood in rivers. Earth Surface Processes and Landforms (in press)
35. Tang YJ, Xu ZM, Yang TQ, Zhou ZH, Wang K, Ren Z, Yang K, Tian L (2018) Impacts of small woody debris on slurrying, persistence, and propagation in a low-gradient channel of the Dongyuege debris flow in Nu River, Southwest China. Landslides 15:2279–2293
36. Tsuguti H, Seino N, Kawase H, Imada Y, Nakaegawa T, Takayabu I (2019) Meteorological overview and mesoscale characteristics of the Heavy Rain Event of July 2018 in Japan. Landslides 16:363–371
37. Ulloa H, Iroumé A, Mao L, Andreoli A, Diez S, Lara LE (2015) Use of remote imagery to analyse changes in morphology and longitudinal large wood distribution in the Blanco River after the 2008 Chaitén volcanic eruption, southern Chile. Geografiska Annaler: Series A, Physical Geography 97:523–541
38. Wallace JB, Benke AC (1984) Quantification of wood habitat in subtropical coastal plain streams. Canadian Journal of Fisheries Aquatic Science 41:1643–1652
39. Woodsmith RD, Buffington JM (1996) Multivariate geomorphic analysis of forest streams: implications for assessment of land use impact on channel condition. Earth Surf Proc Land 21:377–393
40. Wyżga B, Mikuś P, Zawiejska J, Ruiz-villanueva V, Kaczka RJ, Czech W (2017) Log transport and deposition in incised, channelized, and multithread reaches of a wide mountain river: Tracking experiment during a 20-year flood. Geomorphology 279:98–111

Figures

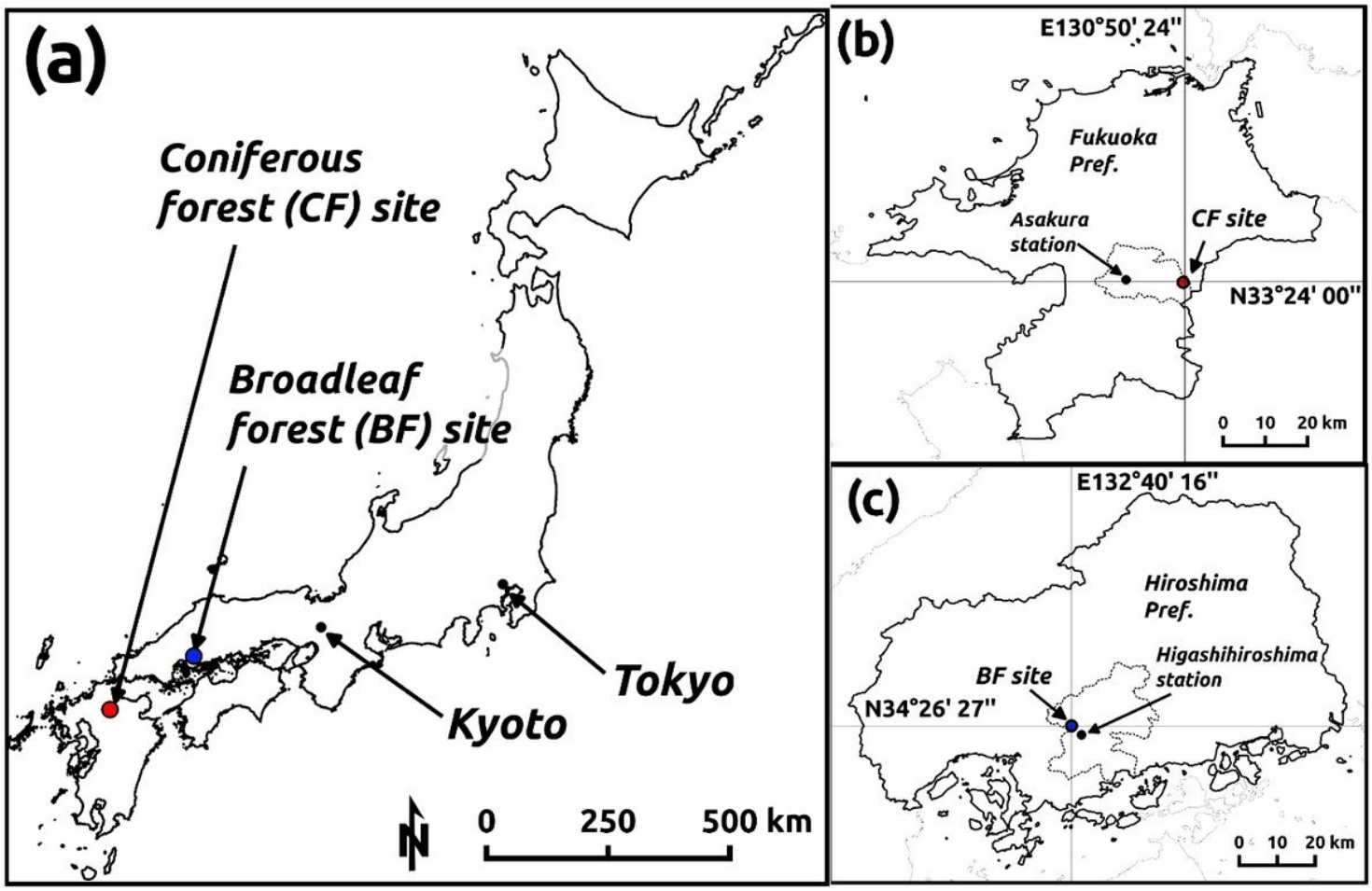

Figure 1

Study site: (a) overview, (b) locations of the coniferous forest (CF) site and the rain-gauge station (Asakura station), and (c) locations of the broadleaf forest (BF) site and the rain-gauge station (Higashihiroshima station).

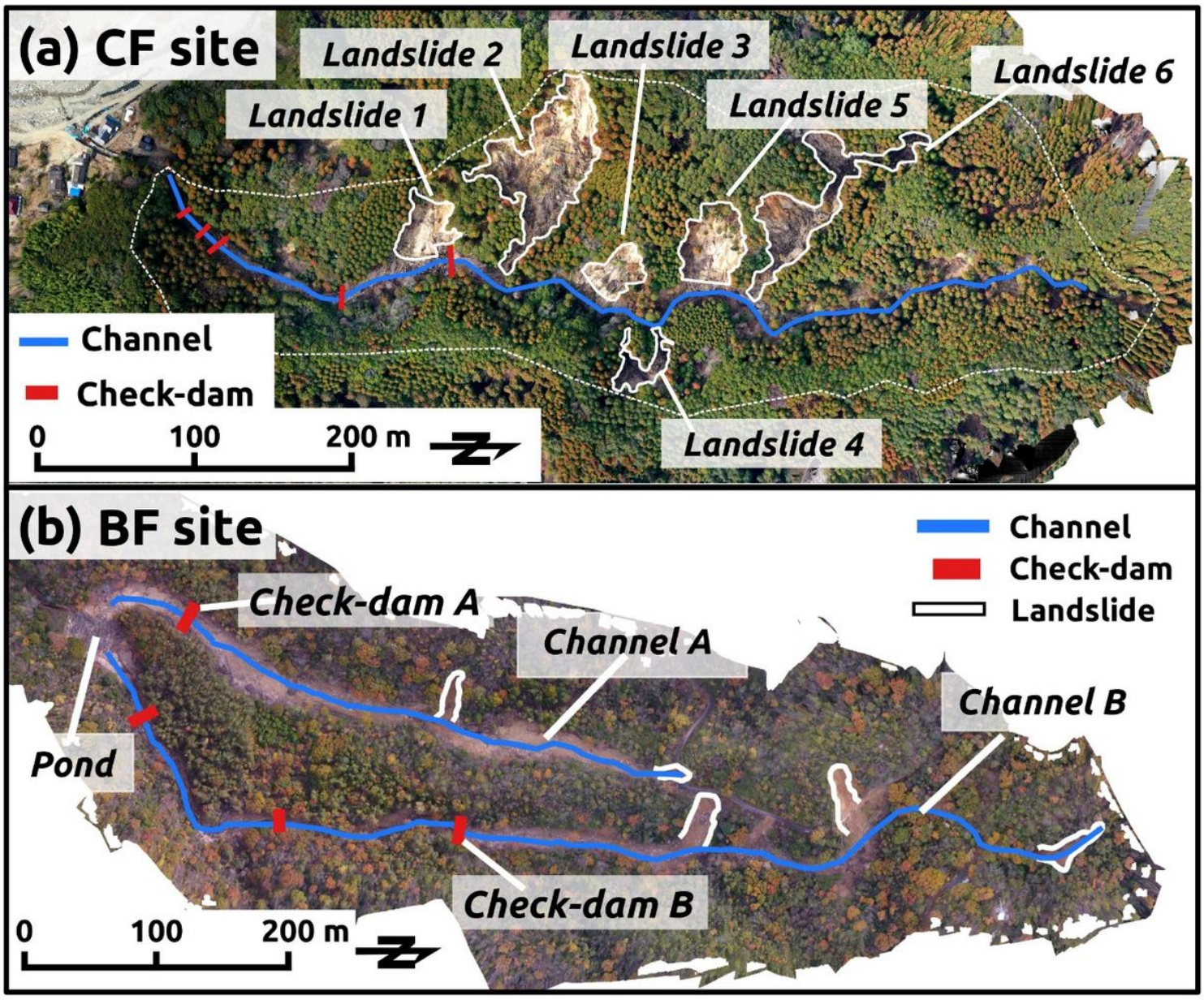

Figure 2

Ortho-photograph of the study sites: (a) the CF site and (b) the BF site. The right side indicates the upper part of the channel (i.e., the streams descend from north to south).

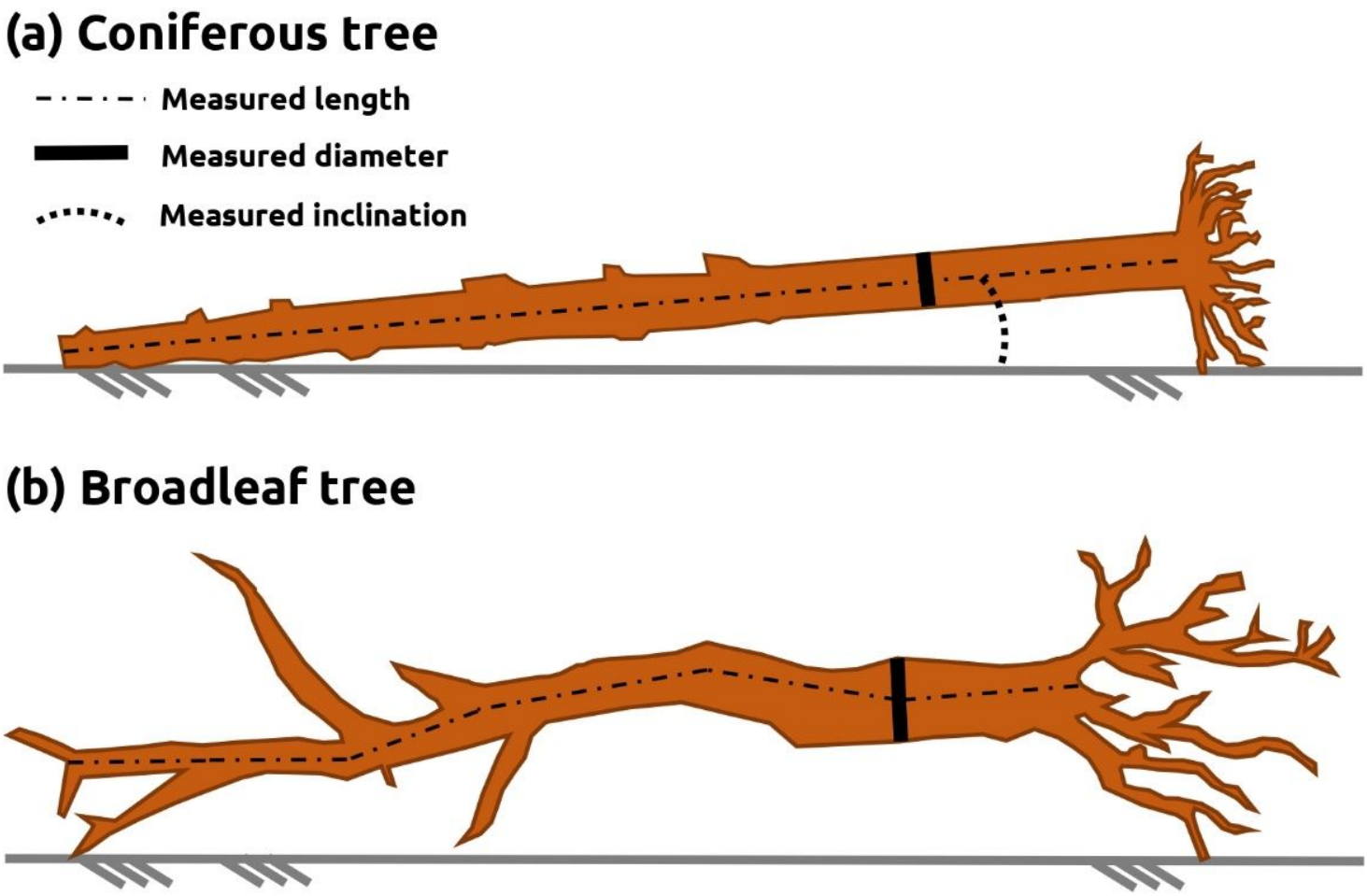

Figure 3

Schematic representation of the components for the direct measurement of woody debris: (a) the coniferous tree and (b) broadleaf tree. The left side indicates the top of the trees (the side of the tree crown). The right side depicts the root-wad.

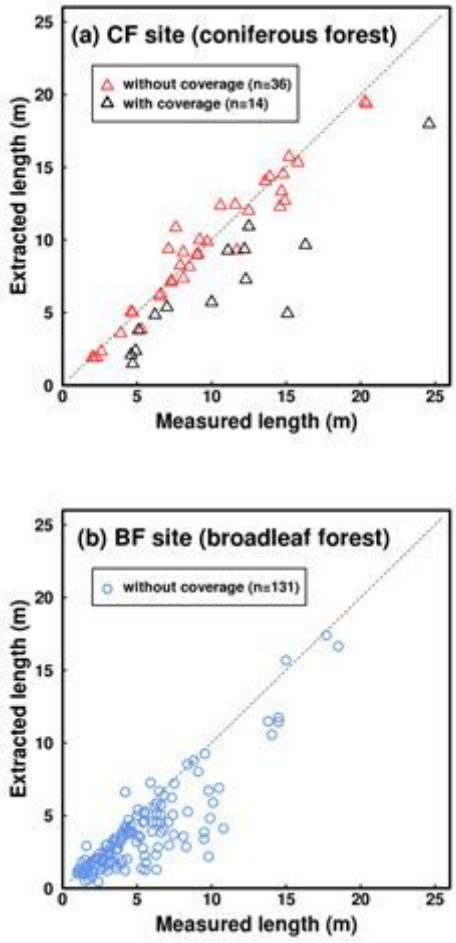

Figure 4

Comparison between extracted and measured length of woody debris: (a) the CF site and (b) the BF site.

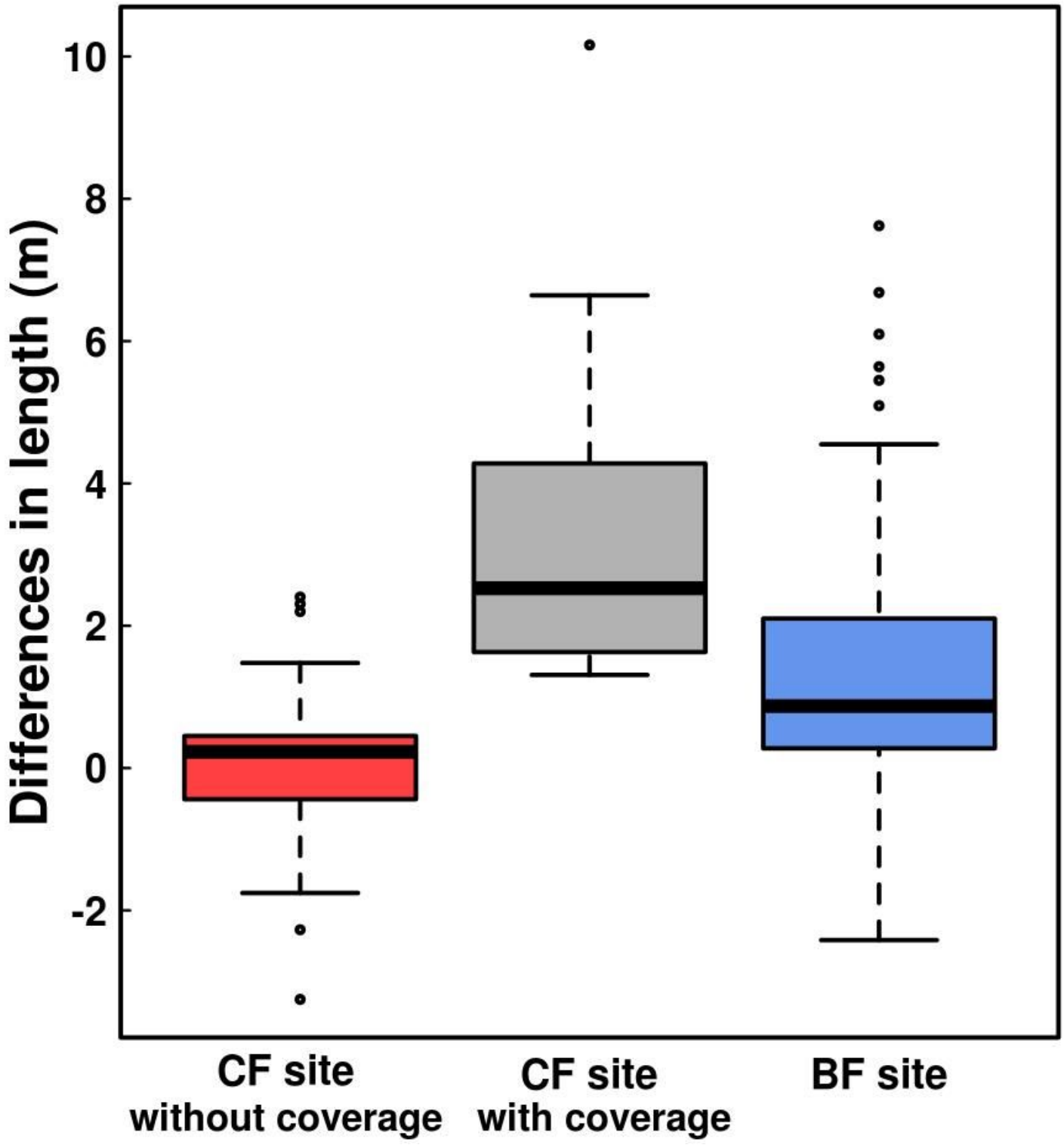

Figure 5

Boxplot of differences between extracted and measured length of the woody debris. Differences in length were calculated by subtracting the extracted length from the measured length.

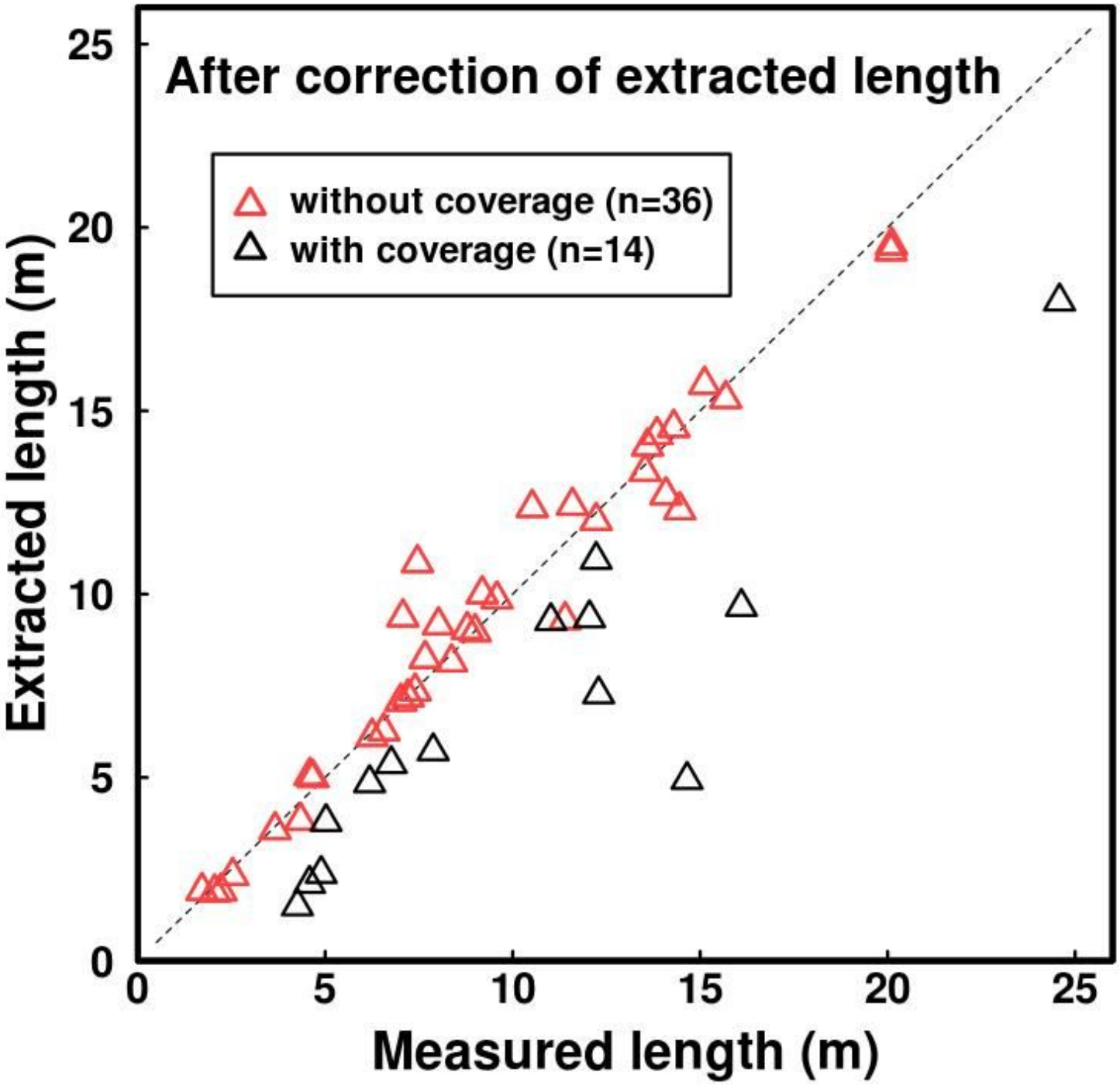

Figure 6

Comparison between corrected extracted length and measured length of the woody debris at the CF site. The corrected extracted length indicates that the inclined length was corrected from the extracted length (i.e., orthogonally projected length) using the directly measured inclination of the woody debris.

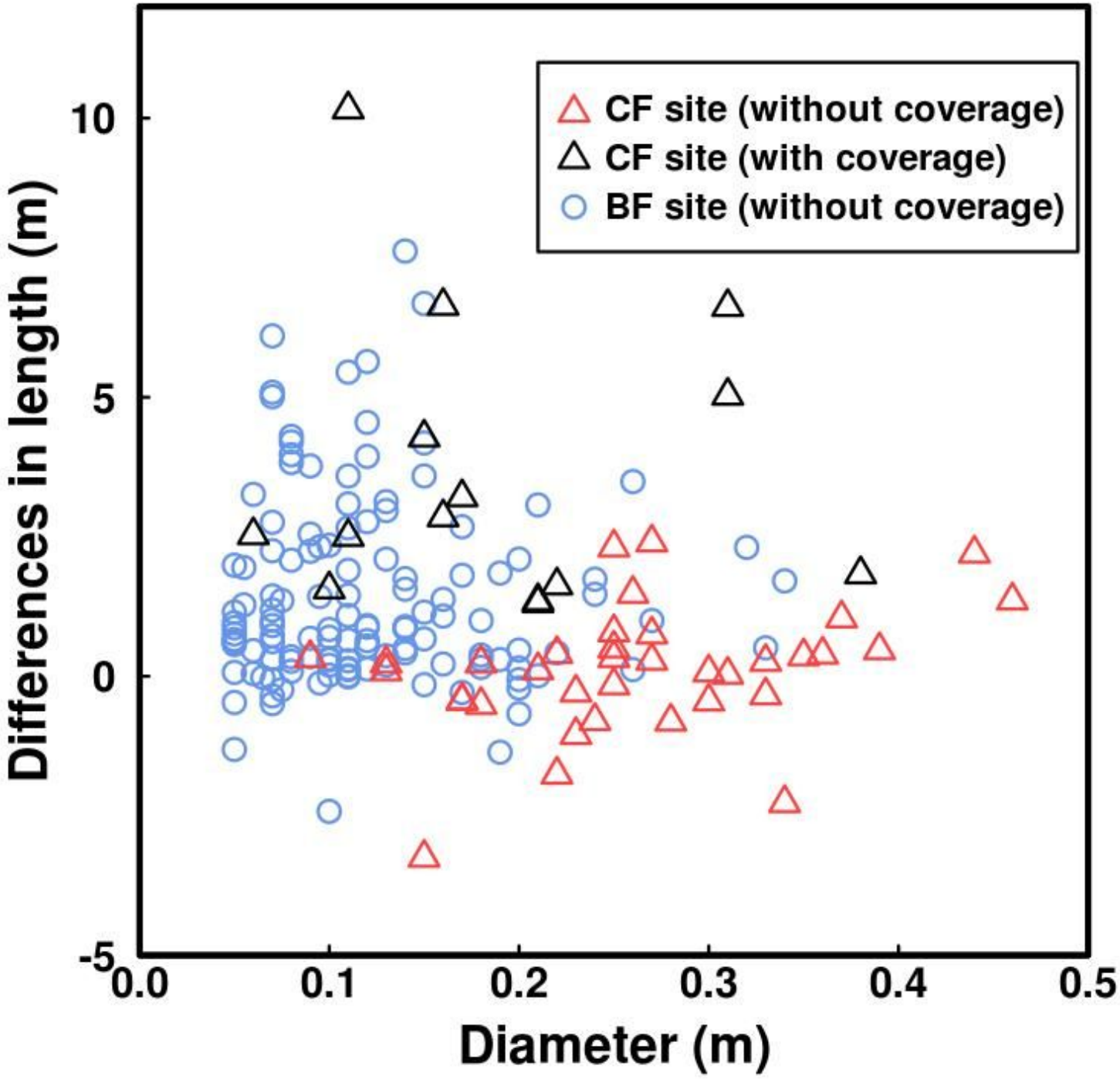

Figure 7

Comparison between measured diameter and differences between extracted and measured length of the woody debris. Differences in length were calculated by subtracting the extracted length from the measured length, similar to Figure 5.

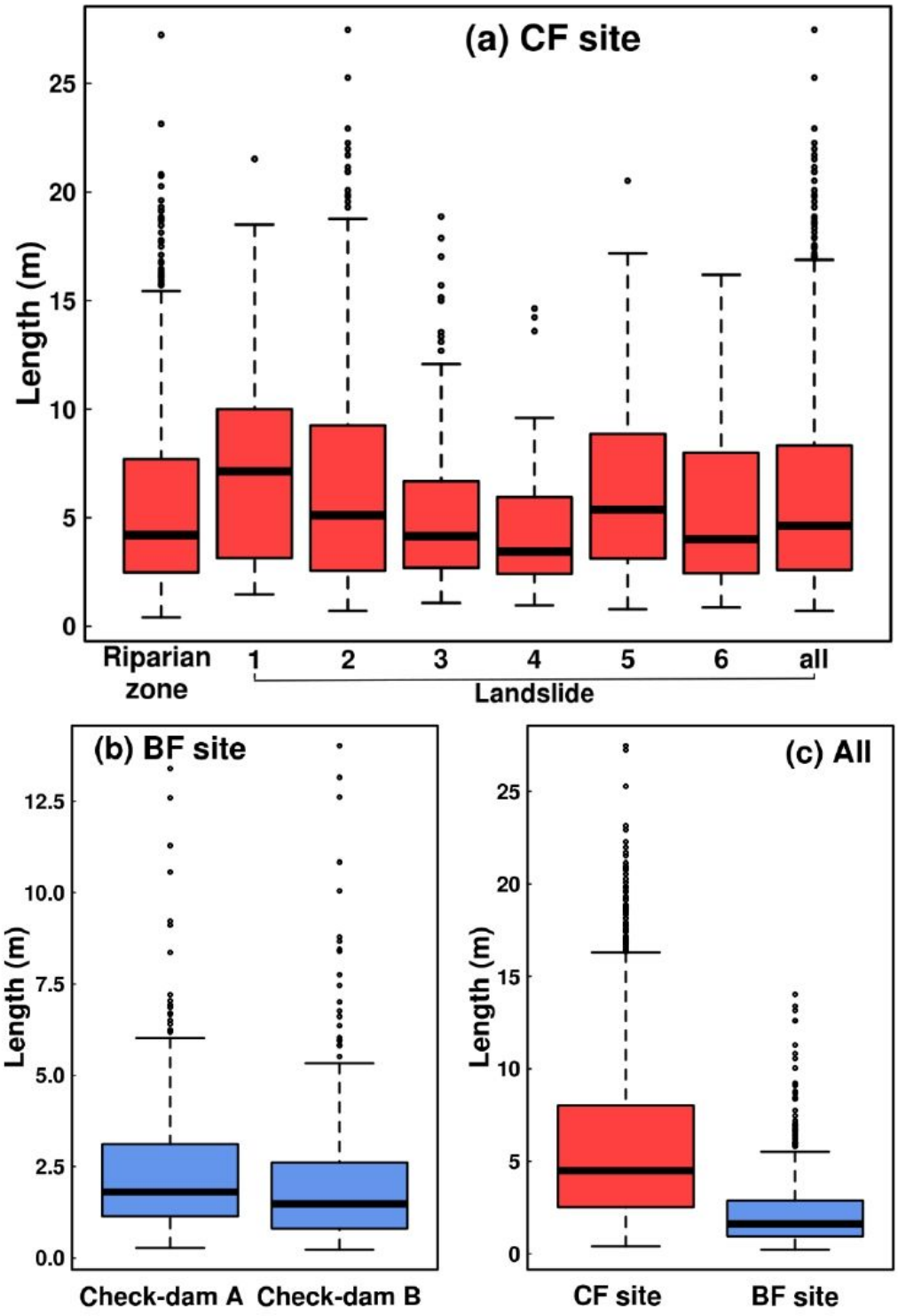

Figure 8

Boxplots of extracted length: (a) the CF site, (b) the BF site, and (c) all measured lengths. In the (a) panel, the label of the landslides corresponds to Figure 2a (all indicates the total number of landslides). The woody debris extracted in the area excluding landslide scars was regarded as the riparian zone (Figure 9).

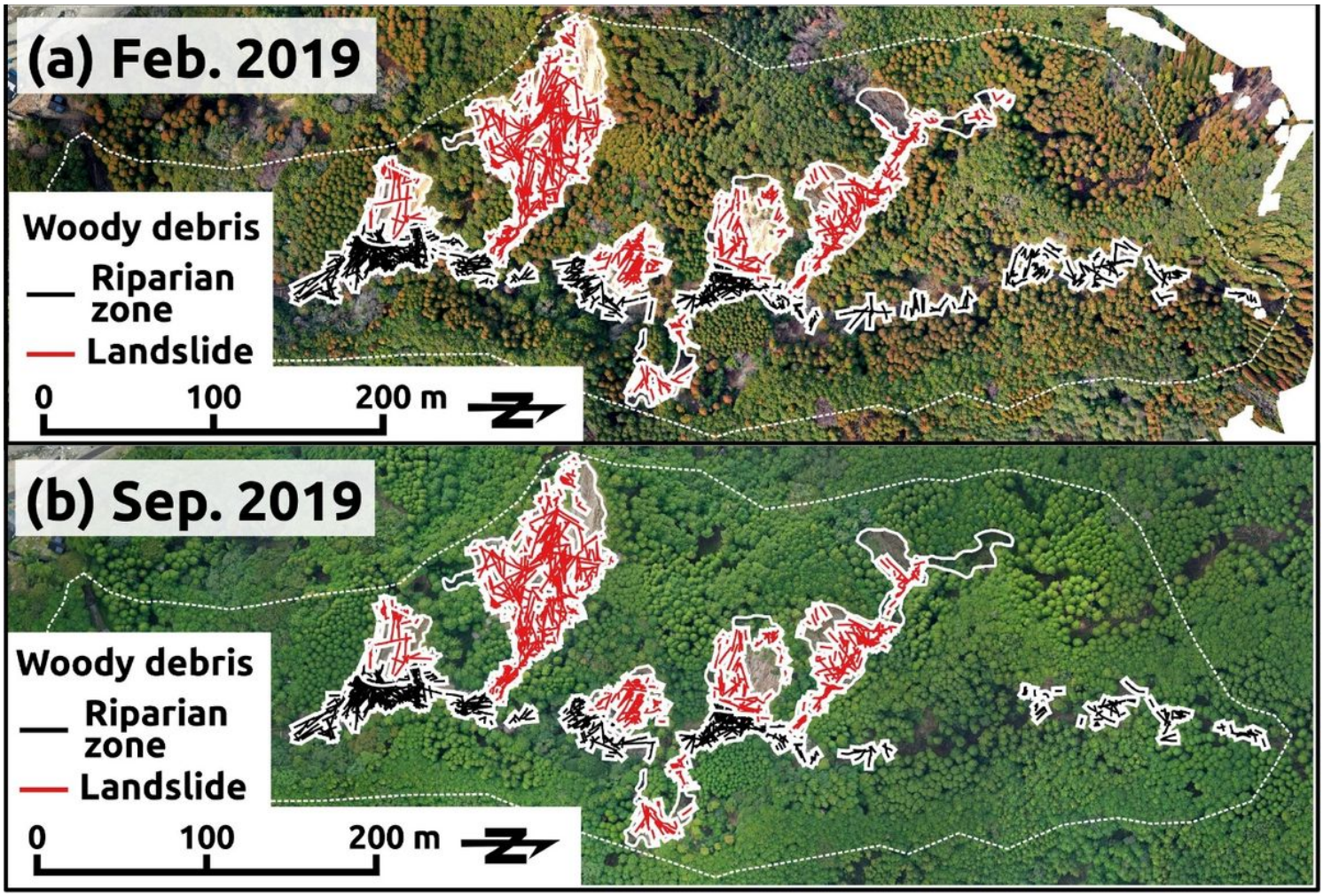

Figure 9

Spatial distribution of extracted woody debris in the CF site: (a) February 14, 2019, and (b) September 26, 2019.

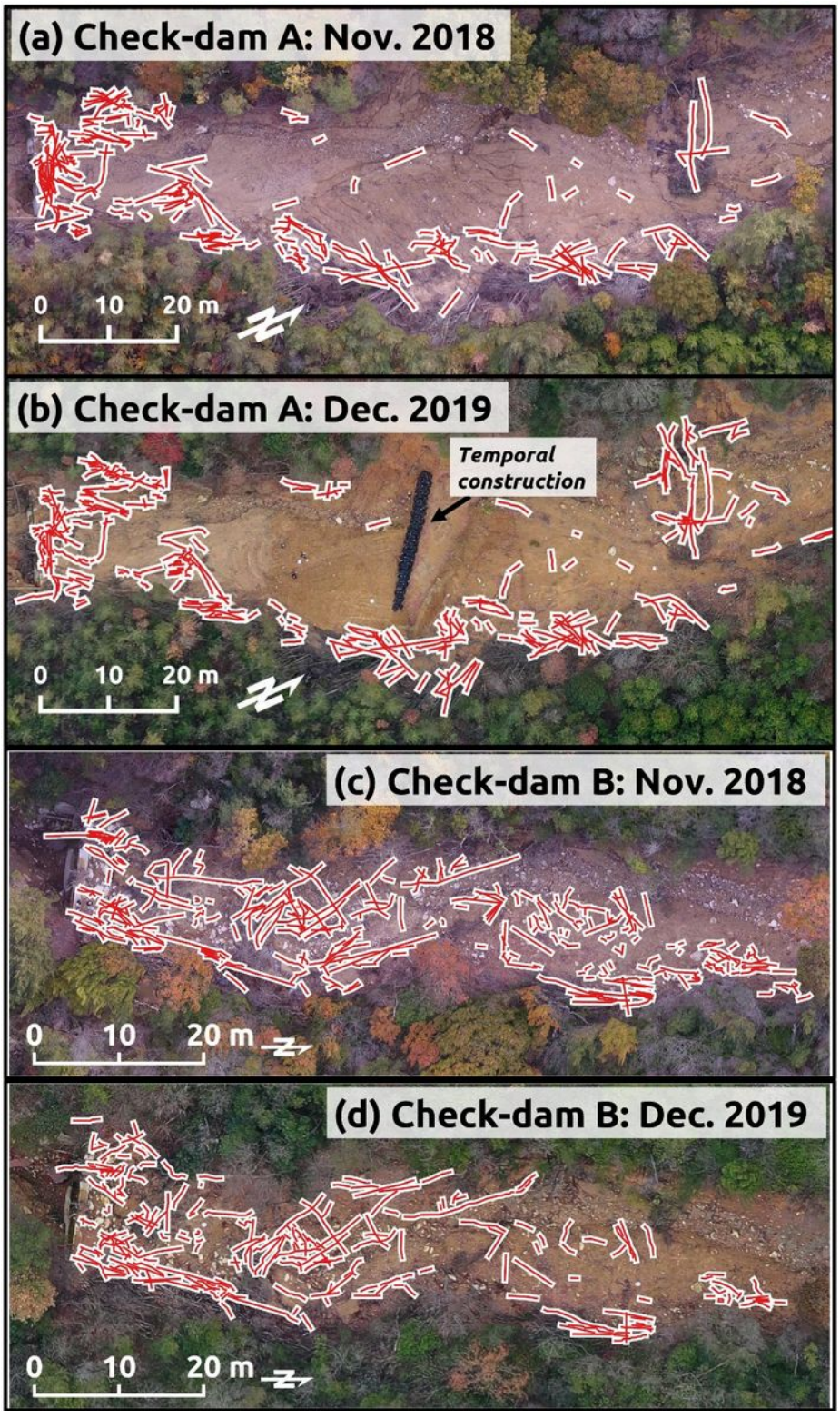

Figure 10

Spatial distribution of extracted woody debris in the BF site: (a) the check-dam A on November 16, 2018, (b) the check-dam A on December 25, 2019, (c) the check-dam B on November 16, 2018, and (d) the check-dam B on December 25, 2019.

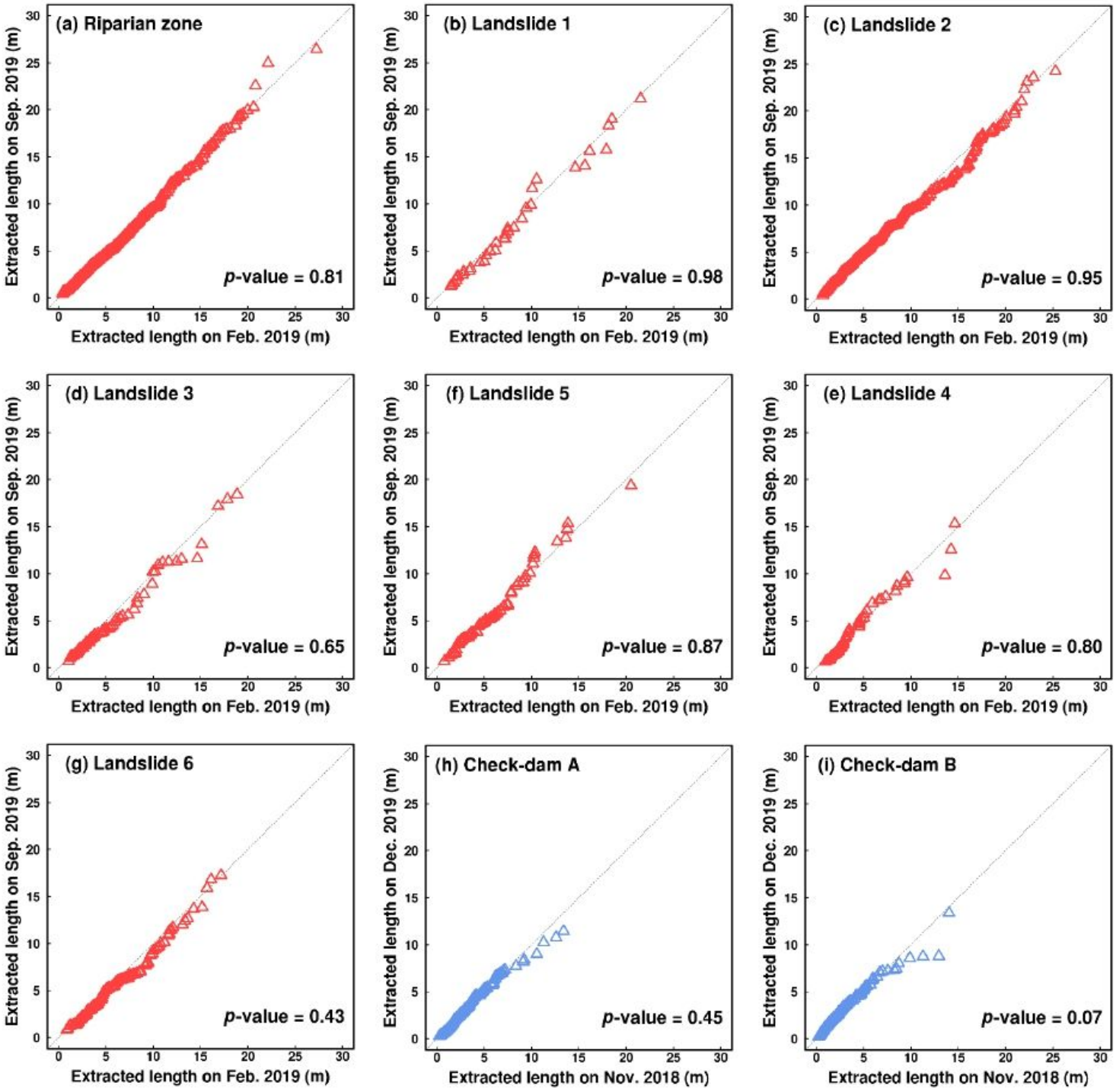

Figure 11

Q-Q plots for the length of extracted woody debris: (a-g) the CF site and (h-i) the BF site. The p-value indicates the result of the goodness-fit-test (the Kolmogorov–Smirnov test).

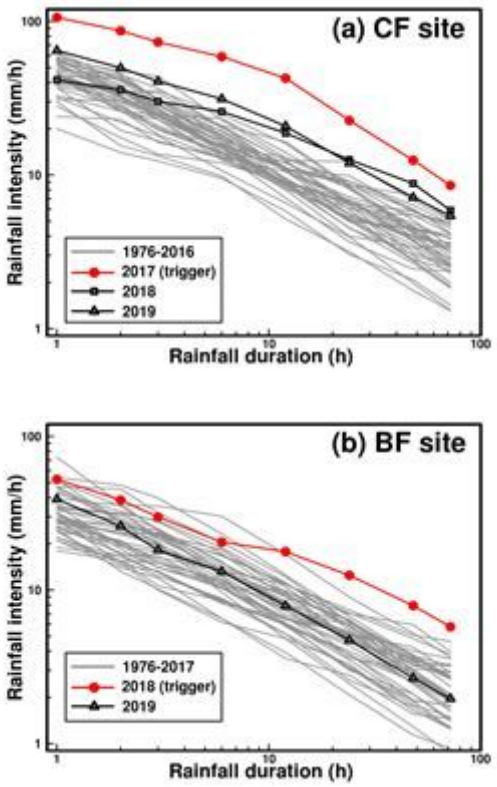

Figure 12

Curves for annual maxima of rainfall intensity: (a) the CF site and (b) the BF site.

Supplementary Files

This is a list of supplementary files associated with this preprint. Click to download.

- GraphicalAbstract.jpg